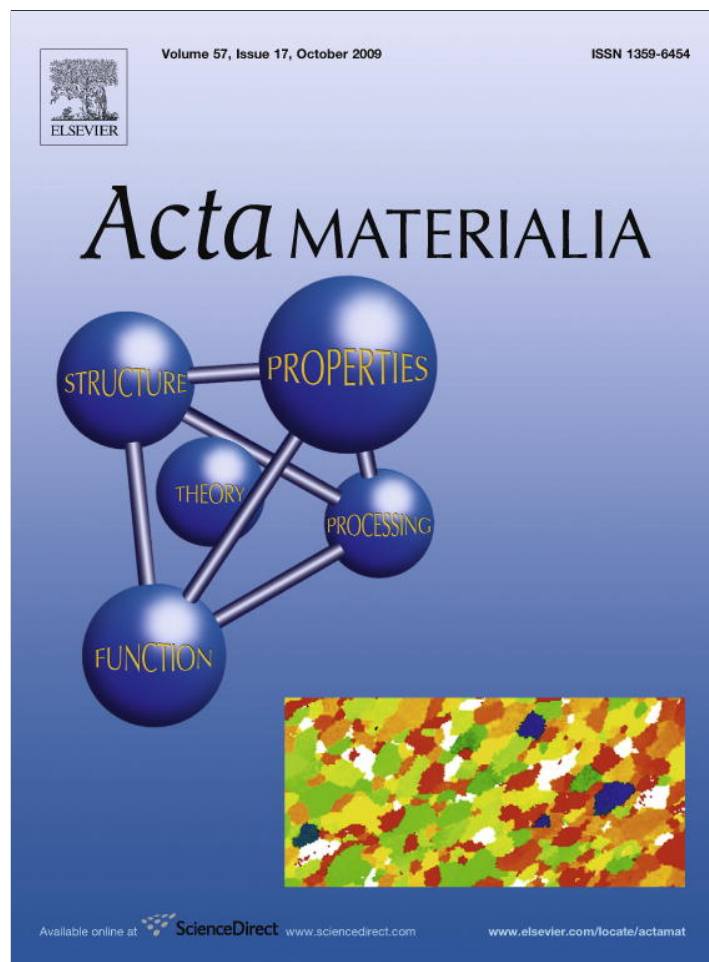


Provided for non-commercial research and education use.  
Not for reproduction, distribution or commercial use.



This article appeared in a journal published by Elsevier. The attached copy is furnished to the author for internal non-commercial research and education use, including for instruction at the authors institution and sharing with colleagues.

Other uses, including reproduction and distribution, or selling or licensing copies, or posting to personal, institutional or third party websites are prohibited.

In most cases authors are permitted to post their version of the article (e.g. in Word or Tex form) to their personal website or institutional repository. Authors requiring further information regarding Elsevier's archiving and manuscript policies are encouraged to visit:

<http://www.elsevier.com/copyright>



# Low-angle grain boundary migration in the presence of extrinsic dislocations

A.T. Lim<sup>a</sup>, D.J. Srolovitz<sup>b</sup>, M. Haataja<sup>a,\*</sup>

<sup>a</sup> Department of Mechanical and Aerospace Engineering, Princeton University, Princeton, NJ 08544, USA

<sup>b</sup> Department of Physics, Yeshiva University, New York, NY 10033, USA

Received 8 June 2009; received in revised form 1 July 2009; accepted 2 July 2009

Available online 17 August 2009

## Abstract

We investigated the migration of a symmetric tilt, low-angle grain boundary (LAGB) under applied shear stress in the presence of extrinsic dislocations. The results demonstrate that there is a threshold stress for the LAGB to depin from extrinsic dislocations. Below the threshold stress, the LAGB remains immobile at zero dislocation climb mobility, while for finite climb mobilities, it migrates at a velocity that is directly proportional to the applied stress, with a proportionality factor that is a function of misorientation, dislocation climb mobility and extrinsic dislocation density. We derive analytical expressions for the LAGB mobility and threshold stress for depinning from extrinsic dislocations. The analytical prediction of the LAGB mobility is in excellent agreement with the simulation as well as experimental results. We discuss the implications of these results for understanding the migration of general grain boundaries.

© 2009 Acta Materialia Inc. Published by Elsevier Ltd. All rights reserved.

**Keywords:** Grain boundary migration; Grain boundary mobility; Dislocation boundaries; Dislocation dynamics

## 1. Introduction

Grain boundary (GB) migration facilitates many important microstructural evolution processes such as recrystallization, grain growth and high-temperature/low-stress deformation of polycrystals. From a theoretical perspective, developing predictive models for the mobility of an arbitrary GB is extremely challenging due to the collective nature of the rearrangement of atomic configurations at the boundary and the constraint placed upon these by the symmetries of the adjoining crystalline grains. While the atomic structure of a general GB is sensitive to both atomic bonding and symmetry constraints, the structure of a low-angle grain boundary (LAGB) is relatively simple [1]. LAGBs consist predominantly of (elastically distorted) perfect crystal regions and an array of lattice dislocations. Because LAGBs are structurally much simpler than general GBs, a complete understanding of the migration of LAGBs

should be much simpler to achieve than for general GBs—after all, LAGB migration should be describable in terms of the collective motion of the dislocation array that makes up the LAGB.

In the present study, we focus on the migration of LAGBs. LAGBs were first analyzed by Burgers [2] and Bragg [3], and observed in Ge crystals grown from seeded melts by Vogel et al. [4]. Because such boundaries consist of lattice dislocations, we should expect LAGBs to migrate when a shear stress is applied such that the Peach–Köhler force on the constituent dislocations is non-zero. Based upon these ideas, a symmetric tilt LAGB, consisting of parallel edge dislocations with the same Burgers vector  $\mathbf{b}$ , is expected to migrate under an applied shear stress  $\tau$  with a velocity  $v_{GB} = m_g \tau b$  [5–7] for  $\tau$  greater than the Peierl's stress (where  $m_g$  is the dislocation glide mobility), regardless of temperature and misorientation  $\theta$ . This suggests that LAGB mobility should be nearly athermal and scale as  $1/\theta$ . However, studies of stress-induced migration of LAGBs in Zn [8,9] show that the LAGB mobility is temperature dependent and decreases with increasing misorientation,

\* Corresponding author.

E-mail address: [mhaataja@princeton.edu](mailto:mhaataja@princeton.edu) (M. Haataja).

contrary to expectation. More recently, Winning et al. used an applied stress to induce the motion of planar, symmetric tilt LAGBs [10,11]. Their measured LAGB mobilities as a function of temperature led to the suggestion that LAGB migration is associated with climb-assisted motion of the lattice dislocations that comprise the boundary.

The motion of GBs in real materials is complicated by the interaction of GBs with a plethora of other defects, such as lattice dislocations, vacancies, interstitials, solutes/impurities and precipitates. Defects such as lattice dislocation and vacancies are always present and therefore it is not always possible to separate GB dynamics from those of other defects. These contribute to what may be thought of as the intrinsic boundary mobility. For example, Rollett [12] suggests that the rate of migration of symmetric tilt LAGBs is controlled by vacancy diffusion to and from “extrinsic” or redundant dislocations. These “extrinsic” dislocations are redundant in the sense that they are not geometrically necessary, i.e. they do not contribute to the overall misorientation of the GB (e.g. these could be part of an array of lattice dislocations provided that there is an equal density of both signs of the same Burgers vector). Hence, it is possible to separate the effects of misorientation (and the “intrinsic” dislocations that contribute to it) from “extrinsic” dislocations (that make no net contribution to misorientation). Such a separation is appropriate here, where our main goal is the development of a picture of LAGB migration based on a dislocation-level description.

In the present study, we focus on the migration of LAGBs in the presence of extrinsic dislocations. These extrinsic dislocations interact directly with the boundary structure and influence the mechanism of LAGB migration. The goal of this work is to develop a mechanistic understanding of how the simplest grain boundaries (i.e. LAGBs), migrate in the presence of extrinsic dislocations. Such a system is simple compared with the migration of general GBs in real materials. Nevertheless, it is both simple enough for a thorough analysis and yet rich enough to include an extrinsic feature that may control the overall mobility of GBs. In this paper, we drive a symmetric tilt boundary with an applied stress and investigate how extrinsic dislocations affect boundary motion. The variables examined here include the magnitude of the driving force (applied stress), dislocation climb mobility, GB misorientation and extrinsic dislocation density.

The rest of this paper is organized as follows. In the next section we present our simulation model, while Section 3 contains results from numerical simulations. The analysis of the results is presented in Section 4 and a detailed comparison with experiments is made in Section 5. The paper concludes with a discussion in Section 6.

## 2. Simulation model

In the present study, we simulate the migration of an ideal, symmetric tilt GB, described as an array of straight, parallel edge dislocations. We investigate the interaction of this LAGB with a set of extrinsic dislocations of Burgers

vectors different from those that make up the boundary itself, but with line directions parallel to those with which the original boundary is composed. In our model, the intrinsic dislocations are those necessary to describe the misorientation between two adjacent grains, while the extrinsic dislocations have net zero Burgers (i.e. equal density of dislocations with opposite Burgers vector) and hence do not contribute to the overall misorientation. In order to study GB migration, we apply a stress that couples to the GB dislocations such that they glide, and thereby translate the GB. The Burgers vectors of the extrinsic dislocations are such that these dislocations must climb in order to keep up with the migrating boundary.

The edge dislocations comprising the boundary have a uniform spacing  $D_1$ , Burgers vector  $\mathbf{b}_1 = \frac{a}{2}[110]$  and line direction  $\xi = [1\bar{1}2]$ , where  $a$  is the lattice constant of the cubic crystal. The Burgers vector of the intrinsic dislocations  $\mathbf{b}_1$  is perpendicular to the boundary plane. The misorientation  $\theta$  is given by

$$\theta = \frac{b_1}{D_1}. \quad (1)$$

Clearly, this GB satisfies Frank's formula [1] and has no long-range stress field.

Next, we introduce a regular array of pairs of extrinsic dislocations with Burgers vectors  $\mathbf{b}_2 = \pm \frac{a}{2}[\bar{1}10]$  that lie within the GB plane. Extrinsic dislocations of the same sign are spaced a distance  $D$  apart and are separated from their oppositely signed nearest neighbors by a distance  $D_2 = D/2$ . The net Burgers vector of the extrinsic dislocation array is zero, such that these dislocations do not contribute to the GB misorientation, nor do they produce long-range stresses (as required by Frank's formula).

There are  $N_1$  intrinsic dislocations in the simulation cell, such that  $\theta = b_1/D_1 = b_1 N_1/D$ . In the present simulations, we set  $4 \leq N_1 \leq 40$  corresponding to misorientations in the range  $0.8^\circ \leq \theta \leq 8.1^\circ$ , which is well within the LAGB regime (i.e. the dislocation separation is much larger than the dislocation core size  $r_0 \approx 0.5a$ ). The extrinsic dislocations are located between two intrinsic dislocations. We fix  $D = 200a$  in our simulations, so that  $D_2 = D/2$  is sufficiently large to ensure that the attraction between the extrinsic dislocations is much smaller than those between the extrinsic and nearby intrinsic dislocations. The extrinsic dislocation/LAGB (intrinsic dislocation) geometry within a simulation unit cell is shown in Fig. 1. This unit cell is periodic along the  $y$ -direction with the dislocations lines oriented along the  $z$ -direction to yield a dislocation array of infinite extent in  $y$  and  $z$ .

The dislocations in the planar boundary configuration were allowed to relax to their equilibrium positions before being subjected to a constant shear stress  $\tau$  along the  $[110]$  direction on the  $(\bar{1}11)$  plane, as shown in Fig. 1. Because these straight, parallel dislocations will remain straight in the absence of interactions with other defects, the migration of this symmetric tilt LAGB is a problem in two spatial dimensions. The position of each dislocation is completely

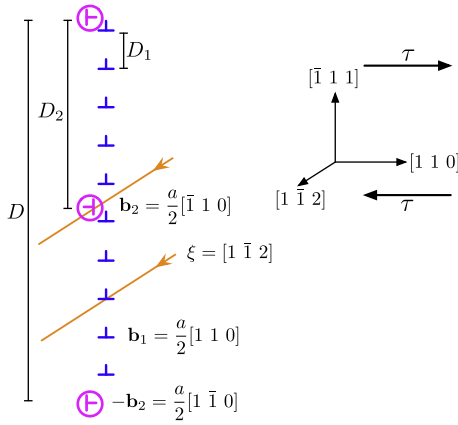


Fig. 1. Schematic illustration of a simulation unit cell for a planar, symmetric LAGB made up of a uniform array of straight, parallel dislocations of lattice Burgers vector  $\mathbf{b}_1$ , in the presence of a widely spaced, parallel extrinsic dislocation array  $\pm\mathbf{b}_2$ . The unit cell is periodic in the  $y$ -direction and of length  $D$  in this direction, such that it contains one pair of oppositely signed extrinsic dislocations, i.e.  $D_2 = D/2$ . The applied shear stress  $\tau$  acts on the  $(\bar{1}11)$  plane in the  $[110]$  direction. In this example,  $D_1 = 20a$  and  $D_2 = 100a$ , such that  $\theta = 2.0^\circ$ .

described by two scalars and the dislocation dynamics is simply the time evolution of these dislocation positions under the action of an applied stress  $\tau$  and the stress fields of all of the dislocations (and their periodic images)  $\sigma^{array}$ .

We evaluate the total stress  $\sigma$  on each dislocation using the stress field summation methods described in Ref. [13] for an isotropic elastic material with shear modulus  $\mu$  and Poisson ratio  $\nu = 1/3$ . The total stress at the position of any dislocation is the sum of contributions from the applied stress and that associated with all other dislocations in the array. Therefore, the total stress on the  $i$ th dislocation at position  $(x_i, y_i)$  in a unit cell of  $N$  dislocations is

$$\sigma_i = \tau + \sigma_i^{array}, \quad (2)$$

where

$$\sigma_i^{array} = \sum_{\substack{j=1 \\ j \neq i}}^N \sigma_i^j \quad (3)$$

and  $\sigma_i^j$  is the stress at the location of the  $i$ th dislocation contributed by the  $j$ th dislocation at position  $(x_j, y_j)$  in the unit cell and its periodic images.

The stress  $\sigma_i^{array}$  tends to infinity as the separation between the  $i$ th and the  $j$ th dislocation approaches zero, because  $\sigma_i^j$  contains terms proportional to  $(\cosh X_{ij} - \cos Y_{ij})^{-2}$  and  $(\cosh X_{ij} - \cos Y_{ij})^{-1}$ , where  $X_{ij} = 2\pi(x_j - x_i)/D$  and  $Y_{ij} = 2\pi(y_j - y_i)/D$ , all of which are singular at  $X_{ij} = Y_{ij} = 0$ . To remove the stress field singularity arising from these terms, we regularize  $\sigma_i^{array}$  by replacing every occurrence of  $(\cosh X_{ij} - \cos Y_{ij})$  in the denominator by  $(\cosh X_{ij} - \cos Y_{ij} + \delta)$ , where  $\delta = 2\pi\epsilon/D$  is a small dimensionless number and  $\epsilon$  has dimension of length (of course, we require that  $\epsilon \ll D_1$ ). Here,  $\epsilon$  plays the role of the dislocation core radius  $r_0$  and is set to  $\epsilon = 0.5a$ .

The Peach–Kohler force on the  $i$ th dislocation of Burgers vector  $\mathbf{b}_i$  and line direction  $\hat{\xi}$  is

$$\mathbf{f}_i = \boldsymbol{\sigma}_i \cdot \mathbf{b}_i \times \hat{\xi}. \quad (4)$$

We assume that the motion of each dislocation is overdamped [14], such that its velocity is proportional to the Peach–Kohler force

$$\mathbf{v}_i = \mathbf{M}_i \cdot \mathbf{f}_i, \quad (5)$$

where  $\mathbf{M}_i$  is a tensor that represents the different mobilities of dislocations in the glide and climb directions. Assuming that the glide mobilities of edge and screw dislocations are identical,  $\mathbf{M}_i$  may be written as

$$\mathbf{M}_i = m_g(\mathbf{I} - \mathbf{n}_i \otimes \mathbf{n}_i) + m_c(\mathbf{n}_i \otimes \mathbf{n}_i), \quad (6)$$

where  $\mathbf{I}$  is the identity matrix,  $m_g$  and  $m_c$  are the glide and climb mobilities, and  $\mathbf{n}_i$  is the glide plane normal of the  $i$ th dislocation, respectively. For a pure screw dislocation, the expression for the mobility reduces to  $\mathbf{M}_i = m_g \mathbf{I}$ . The equations of motion for all dislocations in the unit cell are integrated numerically using an adaptive, fourth-order Runge–Kutta method.

### 3. Results

In the absence of extrinsic dislocations, the uniformly spaced intrinsic dislocations that make up the initially planar, symmetric, LAGB is mechanically stable, i.e. the intrinsic dislocations are already in their stable equilibrium positions with respect to climb and glide. The boundary remains planar and the dislocation spacing  $D_1$  remains constant under relaxation regardless of the value of dislocation climb mobility  $m_c$ . However, the initial dislocation array that makes up the LAGB illustrated in Fig. 1 (i.e. with extrinsic dislocations) is not stable. This is because of the interactions between the intrinsic and extrinsic dislocations. In the absence of an applied stress ( $\tau = 0$ ), the dislocations relax toward their equilibrium positions. During this relaxation,

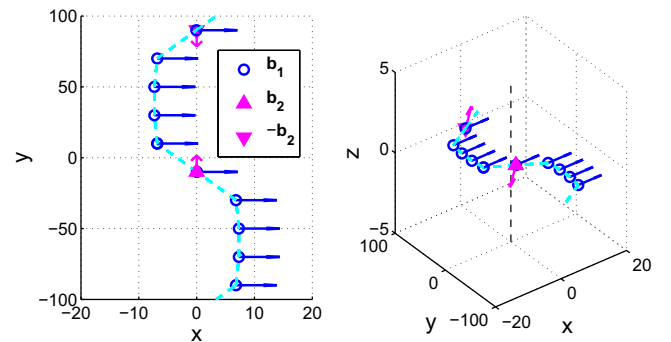


Fig. 2. Dislocation configuration after relaxation with  $m_c = 0$  (positions are shown in units of  $a$ ). The final configurations relaxed at different climb mobilities  $m_c > 0$  are very similar. The dashed line connecting the intrinsic dislocations shows the trace of the LAGB on the  $z = 0$  plane. In the figure on the left, the dislocation lines are directed out of the page. The figure on the right shows a three-dimensional view, indicating the relative positions of the dislocations, and the orientation of the Burgers vectors (indicated by arrows). In simulation coordinates, all of the dislocations are straight and oriented parallel to the  $z$ -axis (indicated by the black dashed line),  $\mathbf{b}_1 = [\frac{1}{\sqrt{2}} 0 0]$ ,  $\mathbf{b}_2 = [0 \frac{1}{\sqrt{3}} \frac{-1}{\sqrt{6}}]$ , and  $\hat{\xi} = [0 0 1]$ .

the extrinsic dislocations glide toward their respective nearest intrinsic dislocations, while the other intrinsic dislocations move away from the mean boundary plane, resulting in an undulating GB, as shown in Fig. 2. (If the extrinsic dislocations are positioned exactly midway between intrinsic dislocations in Fig. 1, the extrinsic dislocations are in unstable equilibrium.) In the course of this relaxation, the extrinsic dislocations displace toward and “merge” or “react” with their respective nearest intrinsic dislocations.

When a constant shear stress  $\tau$  is applied, the intrinsic dislocations that make up the LAGB migrate. The average velocity of these dislocations in the direction normal to the mean boundary plane (i.e. the  $x$ -direction) is the LAGB velocity  $v_{\text{GB}} = \frac{1}{N_1} \sum_{i=1}^{N_1} \dot{x}_i$ . The behavior of the relaxed configuration under the influence of  $\tau$  involves transient rearrangement of relative positions of the intrinsic dislocations (i.e. the LAGB conformation), followed by steady-state migration in the  $x$ -direction. This steady-state migration can be characterized by a fixed LAGB profile (which depends on applied stress  $\tau$  and dislocation climb mobility  $m_c$ , at a fixed misorientation  $\theta$  and extrinsic dislocation separation  $D_2$ ) that moves with a constant velocity  $v_{\text{GB}}$  (a function of  $\tau$ ,  $m_c$ ,  $\theta$  and  $D_2$ ). Henceforth, our discussion on LAGB behavior will refer to its steady-state response, unless otherwise stated.

When the applied stress is low ( $\tau < \tau^*$ ) and the climb mobility is finite ( $m_c > 0$ ), the moving LAGB drags the extrinsic dislocations. For this to happen, the extrinsic dislocations must climb. The overall velocity of the LAGB will be limited by the climb mobility  $m_c$  of the extrinsic dislocations, and therefore  $v_{\text{GB}} < m_g \tau b_1$ . In the limit of zero climb mobility, the LAGB is immobile at low applied stress. At sufficiently high applied stress ( $\tau > \tau^*$ ), the LAGB escapes from the extrinsic dislocations and migrates at  $v_{\text{GB}} = m_g \tau b_1$ , having left behind the dipolar extrinsic dislocation pair; this pair subsequently glides toward each other and annihilates. Fig. 3 illustrates this process for both small and large applied stresses in images shown at uniform time intervals for  $m_c = 0.2m_g$ .

Fig. 4 shows the steady-state GB velocity  $v_{\text{GB}}$  as a function of applied stress  $\tau$  for several values of climb mobility  $m_c$  and misorientation  $\theta$ . For a particular value of  $m_c$  and  $\theta$ ,  $v_{\text{GB}}$  is a piecewise linear function of  $\tau$ . The velocity jumps from a low to high value at an  $m_c$ - and  $\theta$ -dependent threshold or depinning stress  $\tau^*$ . The slope  $dv_{\text{GB}}/d\tau$  for  $\tau < \tau^*$  in Fig. 4 increases with increasing  $m_c$  and  $\theta$ . This implies that for a fixed applied stress, the LAGB migrates faster at higher temperatures, whereas at a fixed temperature, a higher-angle LAGB migrates faster than a lower-angle LAGB (see also Fig. 5); this will be discussed in detail in the next section.

## 4. Analysis

### 4.1. GB velocity and mobility

At steady state (following an initial transient) for  $\tau < \tau^*$ , the simulations show that the LAGB profile remains constant as it migrates in the  $x$ -direction with negligible dis-

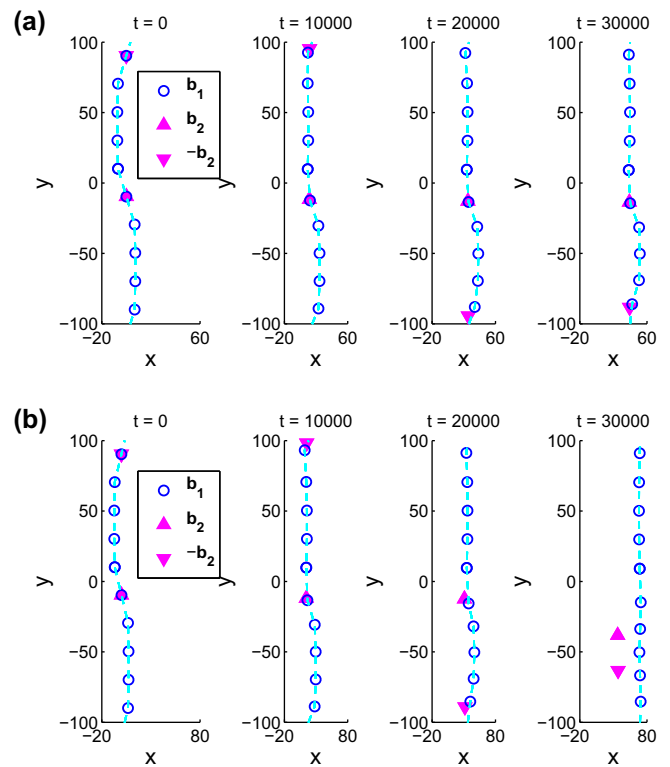


Fig. 3. The spatial arrangement of the intrinsic and extrinsic dislocations at regular time intervals as the LAGB migrates to the right in the simulations with  $m_c = 0.2m_g$  for (a)  $\tau < \tau^*$  and (b)  $\tau > \tau^*$ .

placements of the intrinsic dislocations along the LAGB (i.e. the  $y$ -direction). Let subscripts 1 and 2 refer to intrinsic and extrinsic dislocations, respectively, and superscripts  $g$  and  $c$  to dislocation glide and climb processes, respectively. The glide velocity of an intrinsic dislocation ( $\mathbf{b}_1$ ) is

$$v_1^g = m_g(\tau - \sigma_{1xy})b_1, \quad (7)$$

where  $\sigma_{1xy}$  is the shear stress on the intrinsic dislocation associated with all of the other dislocations in the system. The climb velocity of an extrinsic dislocation ( $\mathbf{b}_2$ ), as it climbs out of its slip plane to keep up with the migrating boundary is

$$v_2^c = m_c(\sigma_{2yy}b_{2y} + \sigma_{2yz}b_{2z}) \simeq m_c\sigma_{2yy}b_{2y}, \quad (8)$$

where  $\sigma_{2yy}$  and  $\sigma_{2yz}$  are normal and shear stresses on the extrinsic dislocation associated with the other dislocations in the system.  $\sigma_{2yz}b_{2z}$  is the force on one extrinsic dislocation ( $\mathbf{b}_2$ ) caused by the other extrinsic dislocation ( $-\mathbf{b}_2$ ). When the separation between the extrinsic dislocations is much greater than that between the intrinsic ones (i.e.  $D_2 \gg D_1$ ), this term is small compared to the force on the extrinsic dislocation associated with the intrinsic dislocations,  $\sigma_{2yy}b_{2y}$ ; hence, it is neglected in the remainder of the present analysis.

The expressions for  $v_1^g$  and  $v_2^c$  contain two unknowns,  $\sigma_{1xy}$  and  $\sigma_{2yy}$ . These stresses are not independent of each other since the velocity of each dislocation must be identical in steady state and equal to the velocity of the migrating LAGB, i.e.  $v_1^g = v_2^c = v_{\text{GB}}$ . This implies

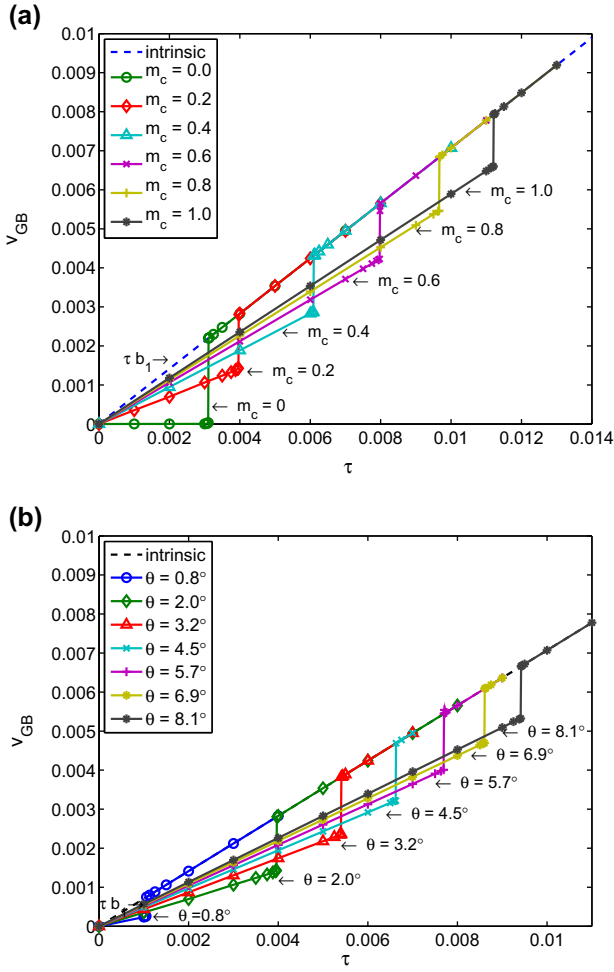


Fig. 4. Steady-state GB velocity  $v_{GB}$  (in units of  $a\mu m_g$ ) as a function of applied shear stress  $\tau$  (in units of  $\mu$ ) for several values of (a)  $m_c$  (in units of  $m_g$ ) at  $\theta = 2.0^\circ$ , and (b)  $\theta$  at  $m_c = 0.2$ . The dashed line indicates the GB velocity as a function of  $\tau$  in the absence of extrinsic dislocations, i.e.  $v_{GB} = m_g \tau b_1$ .

$$m_c \sigma_{2yy} b_{2y} = m_g (\tau - \sigma_{1xy}) b_1. \quad (9)$$

Next we will show that  $\sigma_{1xy} = \beta \sigma_{2yy}$ , where  $\beta$  is a proportionality constant that can be explicitly evaluated by considering the internal (Peach–Kohler) forces on the two types of dislocations (resolved along  $\mathbf{b}_1$ ). To this end, the internal force on the  $m$ th intrinsic dislocation  $f_m$  is the sum of those originating from all other intrinsic dislocations  $f_m^{(i)}$  and extrinsic dislocations  $f_m^{(e)}$  in the array

$$f_m = f_m^{(i)} + f_m^{(e)} = \sum_{\substack{j=1 \\ j \neq m}}^{N_1} f_m^{(i)j} + \sum_{k=1}^{N_2} f_m^{(e)k} = -\sigma_{1xy} b_1, \quad (10)$$

while the internal force on the  $n$ th extrinsic dislocation  $g_n$  is the sum of those originating from all other intrinsic dislocations  $g_n^{(i)}$  and extrinsic dislocations  $g_n^{(e)}$  in the array

$$g_n = g_n^{(i)} + g_n^{(e)} = \sum_{\substack{j=1 \\ j \neq n}}^{N_1} g_n^{(i)j} + \sum_{k=1}^{N_2} g_n^{(e)k} = \sigma_{2yy} b_{2y}. \quad (11)$$

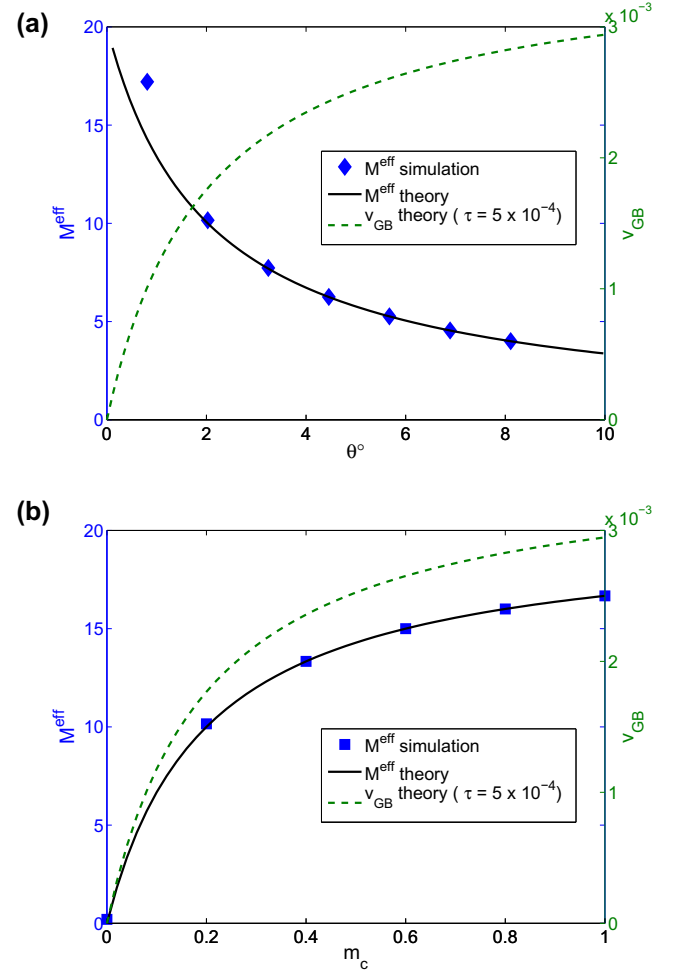


Fig. 5. The effective GB mobility  $M^{eff}$  and velocity  $v_{GB}$  versus (a) misorientation  $\theta$  for fixed climb mobility  $m_c = 0.2$  (in units of  $m_g$ ), and (b) the dislocation climb mobility,  $m_c$  for fixed misorientation  $\theta = 2.0^\circ$ .

Summing over all intrinsic dislocations in Eq. (10) and over all extrinsic dislocations in Eq. (11) yields the net internal forces on the intrinsic and extrinsic dislocations:

$$f_{net}^{(i)} = \sum_{m=1}^{N_1} f_m = \sum_{m=1}^{N_1} \sum_{k=1}^{N_2} f_m^{(e)k} = -N_1 \sigma_{1xy} b_1 \quad (12)$$

and

$$g_{net}^{(e)} = \sum_{n=1}^{N_2} g_n = \sum_{n=1}^{N_2} \sum_{\substack{j=1 \\ j \neq n}}^{N_1} g_n^{(i)j} = N_2 \sigma_{2yy} b_{2y}. \quad (13)$$

Note that the net internal force on the intrinsic dislocations is solely due to the extrinsic dislocations and vice versa—courtesy of Newton's third law. Since  $f_{net}^{(i)} = -g_{net}^{(e)}$  (again from Newton's third law),  $N_2 \sigma_{2yy} b_{2y} = N_1 \sigma_{1xy} b_1$ . Thus, we obtain

$$\sigma_{1xy} = \frac{N_2 b_{2y}}{N_1 b_1} \sigma_{2yy} = \frac{b_{2y}}{D_2 \theta} \sigma_{2yy}. \quad (14)$$

Hence,  $\beta$  is given by

$$\beta(\theta, D_2) = \frac{b_{2y}}{D_2\theta}. \quad (15)$$

We can now solve for the original two unknowns  $\sigma_{1xy}$  and  $\sigma_{2yy}$  without resorting to direct summation for pairwise dislocation interactions within the steady-state LAGB profile (this important since the steady-state profile is a priori unknown):

$$\sigma_{1xy} = \frac{\beta\tau}{\beta + \frac{m_c}{m_g} \frac{b_{2y}}{b_1}} = \frac{\tau}{1 + \frac{m_c}{m_g} \frac{D_2\theta}{b_1}}; \quad (16)$$

$$\sigma_{2yy} = \frac{\tau}{\beta + \frac{m_c}{m_g} \frac{b_{2y}}{b_1}} = \frac{\tau}{\frac{b_{2y}}{D_2\theta} + \frac{m_c}{m_g} \frac{b_{2y}}{b_1}}. \quad (17)$$

Using either Eq. (16) in Eq. (7) (or Eq. (17) in Eq. (8)), we now solve for the steady-state LAGB velocity for  $\tau < \tau^*$ :

$$v_{GB} = m_g \left( 1 - \frac{1}{1 + \frac{m_c}{m_g} \frac{D_2\theta}{b_1}} \right) b_1 \tau = m_g^{eff} b_1 \tau. \quad (18)$$

The observation that Eq. (18) is directly proportional to  $\tau$  concurs with simulation results as shown in Fig. 4. Furthermore,  $m_g^{eff}$  in Eq. (18) is the effective dislocation glide mobility of  $\mathbf{b}_1$  in the presence of  $\pm\mathbf{b}_2$ . We can rewrite the LAGB velocity as the product of an effective LAGB mobility  $M^{eff}$  and the applied force per unit area on the LAGB,  $F$ :

$$v_{GB} = M^{eff} F = M^{eff} \frac{\tau b_1}{D_1}. \quad (19)$$

Comparing Eqs. (18) and (19), we find

$$M^{eff} = \frac{m_g^{eff} b_1}{\theta} = \frac{m_g b_1}{\theta} \left( 1 - \frac{1}{1 + \frac{m_c}{m_g} \frac{D_2\theta}{b_1}} \right). \quad (20)$$

Fig. 5 shows  $M^{eff}$  versus both the dislocation climb mobility  $m_c$  and the misorientation  $\theta$ . Clearly, the analytical prediction, i.e. Eq. (20), and the simulation results are in excellent agreement.

The simulated data point corresponding to the smallest value of  $\theta$  in Fig. 5 shows some deviation from the prediction. This is presumably a result of the fact that for  $\theta < 2^\circ$  the density of intrinsic and extrinsic dislocations are comparable. In this limit, the identification of the LAGB structure as a continuous interface rather than as an array of discrete dislocations becomes questionable.

#### 4.2. Threshold stress

The simulation data indicate that the steady state LAGB velocity  $v_{GB}$  undergoes an abrupt jump at  $\tau = \tau^*$ . In this section, we develop an analytical model for the threshold stress  $\tau^*$ . We begin by noting that as long as a steady state exists and the direct interaction between the extrinsic dislocations is negligible, the analysis in the previous section provides accurate analytical expressions for the effective GB mobility  $M^{eff}$  in terms of  $m_c$ ,  $\theta$  and  $D_2$ . We further note that these expressions were derived without directly deter-

mining the forces between dislocations; rather, it was based upon the assumption of steady state and the application of Newton's third law. Indeed, the shape of the boundary never entered the analysis, even though the boundary shape does have a strong influence on the threshold behavior of the LAGB.

Now, the difficulty in developing an accurate theoretical model for the threshold behavior lies in the observation that the local shear stress  $\tau - \sigma_{1xy}$  in Eq. (7) has contributions from both the extrinsic as well as the intrinsic dislocations through the deformation of the boundary, and these two contributions are difficult to separate. Such a separation, however, is possible within two simplified scenarios: (1) extrinsic dislocation exerts only a localized pinning force on the nearest intrinsic dislocation, and (2) extrinsic dislocations exert the same pinning force on all intrinsic dislocations. The first scenario, appropriate at small  $\theta$ , is amenable to the classical bow-out analysis, where the LAGB is modeled as a continuous interface pinned by obstacles (extrinsic dislocations). The second scenario, in turn, is appropriate at large  $\theta$ , and admits simple solutions as the boundary deformation can be ignored.

We first focus upon scenario (1). Suppose the boundary is a continuous surface with surface tension  $\gamma_{GB}$  and mobility  $M = m_g b_1 / \theta$ , under an external force per unit area  $f_{line} = \tau b_1 / D_1$  acting on the boundary. The boundary migration is resisted by a regular array of cylindrical obstacles with spacing  $D_2$  and mobility  $m_c$ . At steady-state,  $v_{GB} = M(f_{line} - f_{pin}/D_2) = m_c f_{pin}$ , where  $f_{pin}/D_2$  denotes the pinning force per unit area exerted on the boundary by the obstacles. Thus,

$$f_{pin} = \frac{M f_{line}}{M/D_2 + m_c} = \frac{\tau b_1 D_2 / D_1}{1 + \frac{D_2 \theta}{b_1} \frac{m_c}{m_g}} = \frac{\tau D_2 \theta}{1 + \frac{D_2 \theta}{b_1} \frac{m_c}{m_g}} = \sigma_{2yy} b_{2y}. \quad (21)$$

Within the classical bow-out pinning approach in Ref. [15], depinning occurs when  $f_{pin}$  reaches a maximum  $f_{pin}^*$ ;  $f_{pin}^*$  in turn can be related to  $\gamma_{GB}$ , the boundary shape, and  $D_2$  via a force balance at the obstacle:

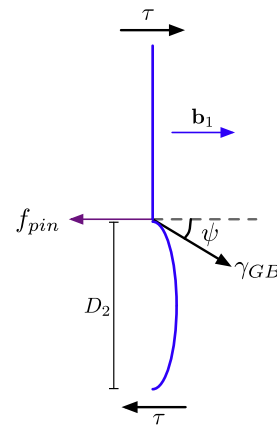


Fig. 6. Schematic illustration of the bow-out geometry used to estimate the threshold stress  $\tau^*$ .

$$\frac{f_{pin}^*}{D_2} = \frac{\tau^* \theta}{1 + \frac{D_2 \theta}{b_1} \frac{m_c}{m_g}} = \frac{\gamma_{GB} \cos \psi^*}{D_2}. \quad (22)$$

Here,  $\psi^*$  denotes the critical bow-out angle as illustrated in Fig. 6. The LAGB energy (surface tension) can be written as (see Ref. [13])

$$\gamma_{GB} = \frac{\mu b_1 \theta}{4\pi(1-\nu)} \left[ \ln \frac{\alpha e}{2\pi} - \ln \theta \right]. \quad (23)$$

Thus,

$$\tau^* = \frac{\mu b_1 \cos \psi^*}{4\pi(1-\nu)D_2} \left( 1 + \frac{D_2 \theta}{b_1} \frac{m_c}{m_g} \right) \left[ \ln \frac{\alpha e}{2\pi} - \ln \theta \right]. \quad (24)$$

This equation predicts a non-monotonic dependence of  $\tau^*$  on misorientation  $\theta$  at finite  $m_c$ , while at  $m_c = 0$ ,  $\tau^*$  should be a monotonically decreasing function of  $\theta$ .

Let us next analyze scenario (2), for which the obstacle–boundary interaction is taken to be long range. In this case, depinning occurs when the pinning force per unit area due to obstacles reaches a critical value:

$$\frac{f_{pin}^*}{D_2} = \frac{\tau^* \theta}{1 + \frac{D_2 \theta}{b_1} \frac{m_c}{m_g}} = f_0^*. \quad (25)$$

Thus, the threshold stress can be written as

$$\tau^* = \frac{f_0^*}{\theta} \left( 1 + \frac{D_2 \theta}{b_1} \frac{m_c}{m_g} \right). \quad (26)$$

In this case, note that  $\tau^* \sim \theta^{-1}$  when  $m_c = 0$ , while at finite  $m_c$ ,  $\tau^* \approx f_0^* D_2 m_c / (b_1 m_g)$  when  $\frac{D_2 \theta}{b_1} \frac{m_c}{m_g} \gg 1$ ; in other words,  $\tau^*$  saturates at large  $\theta$ .

Fig. 7 shows the threshold stress  $\tau^*$  versus dislocation climb mobility  $m_c$  and misorientation  $\theta$  from the simulations and the present analysis, Eq. (24), with  $\psi^* = \pi/4$ . The analytical prediction of  $\tau^*$  as a function of  $m_c$  is in excellent agreement with the simulation data, apart from a small shift, at fixed  $\theta$ . Furthermore, as expected from scenario (1),  $\tau^*$  decreases as  $m_c \rightarrow 0$ . On the other hand, simulation results start to deviate significantly from Eq. (24) in the large  $\theta$  limit.

Eq. (26) predicts that  $\tau^*$  should approach zero in the large  $\theta$  limit for  $m_c = 0$  and should converge to a finite value when  $m_c > 0$ . While the trends in the data are consistent with these predictions, the theoretical models are not sufficiently accurate to provide a more quantitative comparison. This is not surprising, as the extrinsic dislocations interact with the intrinsic ones with forces whose magnitude decays as  $\sim r^{-1}$ , where  $r$  denotes their separation, and thus a single extrinsic dislocation interacts with more than one intrinsic dislocation but less strongly with more distant intrinsic dislocations. The inability of the analytical model in Eq. (24) to match the simulation results for  $\tau^*$  versus  $\theta$  may also be attributed to the failure of the surface tension description of the GB energy in the present case, where the GB is not flat and it is assumed that the critical angle  $\psi^*$  is independent of  $\theta$ . The latter can be corrected by using simulation data for  $\psi^*$  at  $\tau^*$ . However, to do so leads to a prediction that is of little direct use.

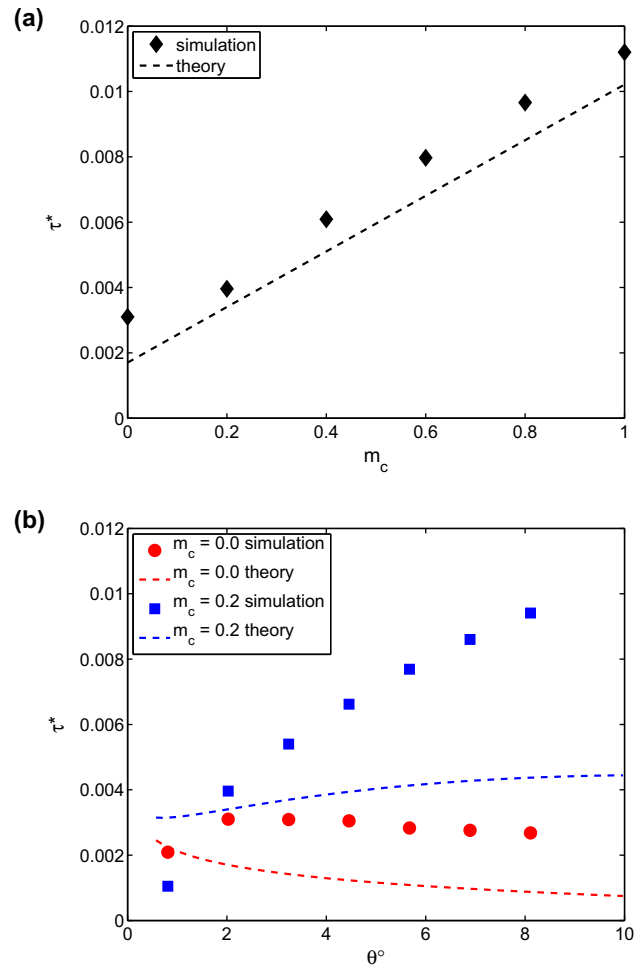


Fig. 7. Threshold stress  $\tau^*$  versus (a) the dislocation climb mobility  $m_c$  for fixed misorientation  $\theta = 2.0^\circ$ , and (b) misorientation  $\theta$  for fixed climb mobility  $m_c = 0.2$  (in units of  $m_g$ ).

## 5. Comparison with experiments

Our analytical and simulation results indicate that the LAGB velocity in the low driving force (stress) regime increases with misorientation  $\theta$ , while the LAGB mobility  $M^{eff}$  for dislocation climb mobility  $m_c = 0.2m_g$  decreases with increasing  $\theta$  at a rate slower than  $1/\theta$  (see Fig. 5). The experimental situation is somewhat murky on the question of the dependence of the GB mobility on misorientation angle: Li et al. [8] and Bainbridge et al. [9] demonstrated that the boundary migration rate decreases with increasing misorientation  $\theta$ , implying a mobility that decreases faster than  $1/\theta$ . In contrast, more recent experiments have shown that GB mobility either increases with misorientation angle [16,17], or is independent of the misorientation angle altogether [10,11].

Given the inconsistencies between the experimental observations from a half-century ago and those from the last decade, we focus on the more recent (and reliable) measurements of Winning et al. [10,11]. Of particular interest is the behavior of  $M^{eff}$  in the limit where  $m_c/m_g \ll 1$ , corresponding to the regime where most experimental measure-

ments of LAGB mobility are made (i.e. at temperatures well below the melting point). Given the excellent agreement between our simulation and analytical results, we analyze this regime within our theoretical framework, where we can treat  $m_c/m_g$  as a continuous variable. Performing a Taylor series expansion of  $M^{eff}$  in Eq. (20) about  $m_c = 0$  yields

$$M^{eff} = m_c D_2 \left[ 1 - \frac{m_c}{m_g} \frac{D_2 \theta}{b_1} + \mathcal{O}(m_c^2) \right]. \quad (27)$$

Note that the leading-order term in this expansion (i.e. the first term in the brackets in Eq. (27)) is independent of  $\theta$ , while the second-order term in  $m_c$  is linear in  $\theta$  with a slope  $-m_c^2 D_2^2 / (m_g b_1)$ . Therefore, Eq. (27) predicts that the LAGB mobility is very nearly  $\theta$ -independent for small  $m_c/m_g$ . This can be seen clearly in Fig. 8, where  $M^{eff}$  (Eq. (20)) is plotted as function of  $\theta$  for several values of  $m_c \ll m_g$ .

We emphasize that  $M^{eff}$  is practically independent of  $\theta$  (at small  $\theta$ ) for physically reasonable values of  $m_c/m_g$  and that this is consistent with the LAGB mobility data obtained by Winning et al. [10,11]. We can estimate the magnitude of  $M^{eff}$  by employing a simple model for  $m_c$  following the approach of Ref. [13]:

$$m_c \simeq \frac{2\pi D_s \Omega}{b_e^2 k_B T \ln(D_2/b_2)}. \quad (28)$$

Here  $D_s = D_0 \exp(-Q/RT)$  is the atomic self-diffusion coefficient,  $\Omega$  the atomic volume,  $b_e$  the edge component of the Burgers vector of the extrinsic dislocations,  $k_B$  the Boltzmann constant, and  $T$  denotes the temperature. We employ physical parameter values appropriate for Al ( $\Omega = 16.60 \text{ \AA}^3$  [18],  $D_0 = 2.25 \times 10^{-4} \text{ m}^2 \text{ s}^{-1}$  and  $Q = 144.4 \text{ kJ mol}^{-1}$  [19]),  $b_e = a/\sqrt{3}$ , and we make a reasonable, yet arbitrary, choice for the extrinsic dislocation spacing  $D_2 = 10^4 a$  (since it enters in a logarithm the results only weakly depend on this choice), where  $a = (4\Omega)^{1/3}$  is the lattice parameter. With these physical parameters, Eq. (27) implies that  $M^{eff} \approx 0.0003, 0.2$  and  $3000 \text{ \mu m s}^{-1} \text{ MPa}^{-1}$  at  $T = 473, 573$  and  $873 \text{ K}$ , respec-

tively. The experiments of Winning et al. [10,11] found the LAGB mobilities at these temperatures to be  $M \approx 0.0003, 0.07$  and  $600 \text{ \mu m s}^{-1} \text{ MPa}^{-1}$ , respectively. The quantitative agreement (within a factor of 5 over the entire temperature range) is remarkable given the rather crude theoretical estimate for  $m_c$ , the absence of adjustable parameters (except for  $D_2$ , which has a very small effect) and the magnitude of the experimental error (see Figs. 11–13 in Ref. [10]). This analysis suggests that these experimental results are consistent with a model in which LAGB mobility is controlled by climb of extrinsic dislocations. (This does not, however, rule out the possibility that other mechanisms (e.g. [11]) may also be important.)

## 6. Discussion

We have performed a series of simulations on the migration of symmetric tilt LAGBs that are driven by an applied stress. Such boundaries were described in terms of a single periodic, uniformly spaced set of well-separated, parallel, edge dislocations with lattice Burgers vectors. The migration of the LAGBs was simulated in terms of a dislocation dynamics method in which the ratio of the dislocation climb and glide mobilities was fixed. We examined LAGB migration as a function of both this mobility ratio and the LAGB misorientation (i.e. intrinsic dislocation separation).

Boundaries of the type described above should be expected to migrate in a nearly athermal manner via pure dislocation glide (a reasonable assumption in the common, but not universal, case where dislocation glide is nearly athermal). On the other hand, GB migration is normally observed to be thermally activated with substantial activation energies [20]. Molecular dynamics (MD) simulations of GBs in pure metals [21–26] invariably show activation energies that are considerably smaller than those measured experimentally. One possible source for this discrepancy is the presence of impurities that interact with the migrating GBs in experiments versus the complete purity of the metals examined in the MD simulations. The effect of impurities on GB mobility has been the subject of many studies [27–35]. Another possible source of the discrepancy between MD simulations and experiments is that in real materials, GBs are never ideal and generally contain extrinsic dislocations (i.e. dislocations that are not geometrically necessary to describe the macroscopic GB misorientation). To model this important case, we introduced extrinsic dislocations into the GBs in our dislocation dynamics simulations of LAGB migration.

The simulations presented above showed that the GB velocity versus driving force (stress) has three main features. At low driving forces, the LAGB velocity is a linear function of the driving force, thereby allowing us to define a GB mobility (i.e. the slope of the velocity versus driving force plot). In the low driving force regime, the GB mobility increased with increasing dislocation climb mobility (at constant glide mobility). As the driving force is increased, an abrupt transition occurs at a critical driving force (or

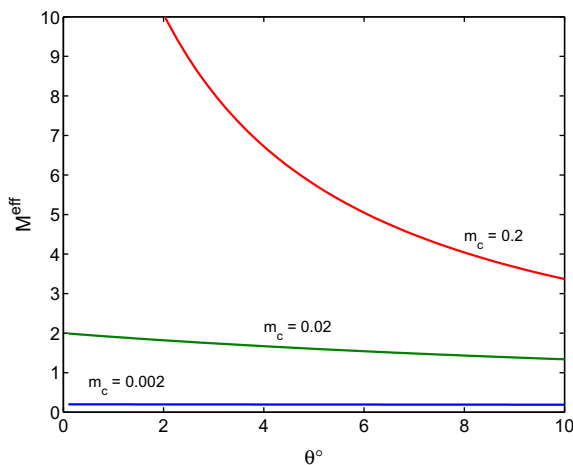


Fig. 8. The effective grain boundary mobility  $M^{eff}$  versus misorientation  $\theta$  for different values of dislocation climb mobility  $m_c$  (in units of  $m_g$ ).

applied threshold stress  $\tau^*$ ) in which the GB velocity jumps from a low velocity to a high velocity. For applied stresses above  $\tau^*$ , the GB velocity is again a linear function of driving force (allowing us to define a high driving force boundary mobility). In this regime, however, the mobility is independent of dislocation climb mobility.

Examination of the dislocation configuration during boundary migration shows that the low driving force regime is characterized by the boundary dragging the extrinsic dislocations, which can only move along with the boundary via climb (hence, the climb mobility dependence of the LAGB mobility in this regime). In this case, the drag created by the extrinsic dislocations makes the LAGB bow-out as it migrates and dominates the activation energy for GB migration. At large driving forces (i.e.  $\tau > \tau^*$ ), the extrinsic dislocations initially retard the LAGB migration, but after a finite time transient, the LAGB pulls away from the extrinsic dislocations and migrates via pure glide of the intrinsic dislocations and in a nearly athermal manner. The low driving force regime is expected to be most common in microstructural evolution.

In the analysis presented in Section 4, we derived an analytical expression for the LAGB mobility in the low driving force regime. This analysis was based upon the action–reaction forces between the intrinsic dislocation array and the extrinsic dislocations, and by requiring that both the intrinsic and extrinsic dislocations move at the same velocity, i.e. the GB velocity. Comparison of the analytical prediction and the simulation results show that the theory accurately describes the LAGB mobility in the low driving force regime, i.e. it properly describes the effect of misorientation, dislocation climb mobility and extrinsic dislocation density. The GB mobility in the high driving force regime was also reproduced by the theory, although this case is the trivial limit of pure dislocation glide (i.e. GB mobility is directly proportional to the glide mobility and inversely proportional to misorientation). Furthermore, we demonstrated that the LAGB mobility is independent of the misorientation to leading order in  $\theta$  for physically reasonable values of the dislocation climb mobility, in excellent qualitative agreement with the LAGB mobility data obtained by Winning et al. [10,11]; quantitatively, our model was able to reproduce the correct order of magnitude of the experimentally observed mobility by employing a classical model for the dislocation climb mobility. A simple analysis was also presented to predict the critical driving force or  $\tau^*$  that was based upon a classic surface tension, bow-out model. Although this bow-out model was able to capture the dependence of  $\tau^*$  on the dislocation climb mobility, it was too crude to accurately reproduce the dependence of  $\tau^*$  on the misorientation, especially at high misorientations. This is likely associated with an assumption in the analysis that the extrinsic dislocations exert only a localized pinning force on the LAGB and that the critical bow-out angle is independent of misorientation. Another simple theoretical model, which assumes that a constant pinning force acts on all intrinsic

dislocations, provides qualitatively reasonable trends at large misorientation.

As discussed in the Introduction, our rationale for focussing upon LAGBs was that they are much simpler structurally than the more common case of general GBs and hence the correlation between dynamic GB structure and migration could be made most precise. As our theoretical analysis has shown, this simplification has led to an accurate, predictive model for GB mobility in the physically important low driving force, low-angle regime. A few observations are in order. First, under normal boundary migration scenarios, the GB mobility of interest is likely to be similar to that in the low driving force limit. Second, the structure of general boundaries is such that pure, athermal glide motion is not possible since general boundaries do not consist solely (or predominantly) of lattice dislocations, but rather of dislocations having Burgers vectors appropriate for the bicrystallography of the situation (i.e. displacement shift complete (DSC) dislocations [36]). In this case, it is both intrinsic and extrinsic dislocations that must climb in order to translate the GB. This means that general GB migration is thermally activated even when no extrinsic dislocations are present. Third, as a GB migrates in a real material, it constantly encounters lattice dislocations. These lattice dislocations can be absorbed into the boundary structure, decaying into DSC dislocations. However, the ability of a GB to continue to absorb dislocations is not limitless. Hence, as the boundary migrates, dislocations may be annihilated within the boundary structure and some dislocations may be emitted behind the moving GB. This implies that the steady-state motion of a general GB in a real material is necessarily a truly dynamic situation. The actual steady-state migration and GB structure may be an ensemble of transient events, such as dislocation adsorption, annihilation and emission.

### Acknowledgements

The authors gratefully acknowledge useful discussions with Anthony Rollett (Carnegie Mellon University). This work has been in part supported by an NSF-DMR Grant No. DMR-0449184 (MH).

### References

- [1] Amelinckx S, Dekeyser W. *Solid State Phys* 1959;8:325–499.
- [2] Burgers JM. *Proc Phys Soc* 1940;52(January):23–33.
- [3] Bragg WL. *Proc Phys Soc* 1940;52(January):54–7.
- [4] Vogel FL, Pfann WG, Corey HE, Thomas EE. *Phys Rev* 1953;90:489–92.
- [5] Chang JP, Bulatov VV, YIP S. *J Comput Aid Mater Des* 1999;6:165–73.
- [6] Chang JP, Cai W, Bulatov VV, Yip S. *Mater Sci Eng A* 2001;309(July):160–3.
- [7] Chang JP, Cai W, Bulatov VV, Yip S. *Comput Mater Sci* 2002;23(April):111–5.
- [8] Li CH, Edwards EH, Washburn J, Parker ER. *Acta Metall* 1953;1(March):223–9.
- [9] Bainbridge DW, Li CH, Edwards EH. *Acta Metall* 1954;2:322–33.

- [10] Winking M, Gottstein G, Shvindlerman LS. *Acta Mater* 2001;49(January):211–9.
- [11] Winking M, Gottstein G, Shvindlerman LS. *Acta Mater* 2002;50(January):353–63.
- [12] Rollett AD. Private communication.
- [13] Hirth JP, Lothe J. *Theory of dislocations*. 2nd ed. Malabar, FL: Krieger; 1992.
- [14] Bulatov VV, Cai W. *Computer simulations of dislocations*. New York: Oxford University Press; 2006.
- [15] Hirth JP. In: Cahn RW, Haasen P, editors. *Physical metallurgy*. Amsterdam: North-Holland; 1996. p. 1831–75 [chapter 20].
- [16] Huang Y, Humphreys FJ. *Acta Mater* 2000;48(May):2017–30.
- [17] Huang Y, Humphreys FJ, Ferry M. *Acta Mater* 2000;48(June):2543–56.
- [18] Steurer W. In: Cahn RW, Haasen P, editors. *Physical metallurgy*. Amsterdam: North-Holland; 1996. p. 1–46 [chapter 1].
- [19] Boucquet JL, Brebec G, Limoge Y. In: Cahn RW, Haasen P, editors. *Physical metallurgy*. Amsterdam: North-Holland; 1996. p. 535–668 [chapter 7].
- [20] Gottstein G, Shvindlerman LS. *Grain boundary migration in metals: thermodynamics, kinetics, applications*. Boca Raton, FL: CRC Press; 1999.
- [21] Schonfelder B, Wolf D, Phillpot SR, Furtkamp M. *Interface Sci* 1997;5(November):245–62.
- [22] Upmanyu M, Smith RW, Srolovitz DJ. *Interface Sci* 1998;6(February):41–58.
- [23] Upmanyu M, Srolovitz DJ, Shvindlerman LS, Gottstein G. *Acta Mater* 1999;47(October):3901–14.
- [24] Zhang H, Mendelev MI, Srolovitz DJ. *Acta Mater* 2004;52(May):2569–76.
- [25] Zhang H, Upmanyu M, Srolovitz DJ. *Acta Mater* 2005;53(January):79–86.
- [26] Zhang H, Mendelev MI, Srolovitz David J. *Scripta Mater* 2005;52(June):1193–8.
- [27] Lucke K, Detert K. *Acta Metall* 1957;5(November):628–37.
- [28] Cahn JW. *Acta Metall* 1962;10(September):789–98.
- [29] Lucke K, Stuwe HP. *Acta Metall* 1971;19(October):1087–99.
- [30] Mendelev MI, Srolovitz DJ. *Boundary motion*. *Acta Mater* 2001;49(February):589–97.
- [31] Mendelev MI, Srolovitz DJ. *Acta Mater* 2001;49(August):2843–52.
- [32] Mendelev MI, Srolovitz DJ, Phil WE. *Mag A* 2001;81(September):2243–69.
- [33] Mendelev MI, Srolovitz DJ. *Interface Sci* 2002;10(April):91–8.
- [34] Mendelev MI, Srolovitz DJ. *Interface Sci* 2002;10(July):191–9.
- [35] Mendelev MI, Srolovitz DJ. *Model Simul Mater Sci* 2002;10(November):R79–109.
- [36] Sutton AP, Balluffi RW. *Interfaces in crystalline materials*. Oxford: Oxford University Press; 2006.